Bioactive Materials 41 (2024) 207–220

Contents lists available at ScienceDirect

Bioactive Materials

journal homepage: www.keaipublishing.com/en/journals/bioactive-materials

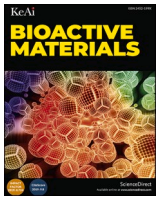

A functional analysis of a resorbable citrate-based composite tendon anchor

Arun Thirumaran [a], Meletios-Nikolaos Doulgkeroglou [a], Magesh Sankar [a], Jeremiah T. Easley [b], Ben Gadomski [b], Anup Poudel [a], Manus Biggs [a,*]

[a] Centre for Research in Medical Devices (CÚRAM), University of Galway, Ireland
[b] Department of Mechanical Engineering, Colorado State University, USA

ARTICLE INFO

Keywords:
Citrate
Osteoinductive
Tendon anchor
Composite

ABSTRACT

Rapid and efficient tendon fixation to a bone following trauma or in response to degenerative processes can be facilitated using a tendon anchoring device. Osteomimetic biomaterials, and in particular, bio-resorbable polymer composites designed to match the mineral phase content of native bone, have been shown to exhibit osteoinductive and osteoconductive properties *in vivo* and have been used in bone fixation for the past 2 decades. In this study, a resorbable, bioactive, and mechanically robust citrate-based composite formulated from poly (octamethylene citrate) (POC) and hydroxyapatite (HA) (POC-HA) was investigated as a potential tendon-fixation biomaterial. In vitro analysis with human Mesenchymal Stem Cells (hMSCs) indicated that POC-HA composite materials supported cell adhesion, growth, and proliferation and increased calcium deposition, alkaline phosphatase production, the expression of osteogenic specific genes, and activation of canonical pathways leading to osteoinduction and osteoconduction. Further, *in vivo* evaluation of a POC-HA tendon fixation device in a sheep metaphyseal model indicates the regenerative and remodeling potential of this citrate-based composite material. Together, this study presents a comprehensive *in vitro* and *in vivo* analysis of the functional response to a citrate-derived composite tendon anchor and indicates that citrate-based HA composites offer improved mechanical and osteogenic properties relative to commonly used resorbable tendon anchor devices formulated from poly(L-*co*-D, L-lactic acid) and tricalcium phosphate PLDLA-TCP.

1. Introduction

Orthopedic therapies have a significantg focus on the stabalization of fractures or bone defects through techniques and devices to promote healing and recovery of bone structure and function. Orthopedic fixation, in particular, relies on mechanically robust and biocompatible screws, anchors, or plate systems to enhance bone stability or promote bone/soft tissue apposition. Advances in materials science have accelerated the development of bioresorbable and bioactive fixation devices, which undergo controlled degradation and regulate the critical processes of osteoinduction, osteoconduction, and osseointegration [1]. In particular, tendon anchoring devices have revolutionized orthopedic surgery, allowing for rapid and efficient tendon fixation to a bone following upper or lower limb joint surgery.

Previous studies into developing effective resorbable fixation devices have reported the use of bioresorbable composite materials, employing a microscale mineral phase dispersed within a polymer matrix. In particular, synthetic polymer composite formulations such as Polycaprolactone (PCL) [2–4], Polymethyl Methacrylate (PMMA) [5,6], Poly-lactic acid (PLA) [7,8], Polyglycolic acid (PGA) [9], their copolymer polylactic-*co*-glycolic acid (PLGA) [10,11], and Poly (glycerol-succinate) (PGS) [12] containing tricalcium phosphate (TCP) or hydroxyapatite (HA) particulates have been extensively described and have seen clinical success as both fixation devices and as scaffolds for regenerative engineering applications [9,13]. Furthermore, recent studies indicate that the chemistry of these materials may be tailored to improve the biocompatibility, mechanical, osteoinductive, and osteoconductive properties of these composite materials *in vitro* and *in vivo* [14–17].

However, there are recognized shortcomings in using synthetic composites as orthopedic materials, specifically related to their manufacturing processes, bioactivity, immunogenicity, biosorption, and osteoinductive capacity. Addressing the limitations of current composite materials in manufacturing orthopedic fixation devices, citrate-based

Peer review under responsibility of KeAi Communications Co., Ltd.
* Corresponding author.
E-mail address: manus.biggs@universityofgalway.ie (M. Biggs).

https://doi.org/10.1016/j.bioactmat.2024.06.030
Received 8 January 2024; Received in revised form 21 June 2024; Accepted 21 June 2024
Available online 22 July 2024

elastomeric composites have been identified as alternative resorbable and biocompatible materials [19–22] with mechanical properties comparable to human cortical bone [18]. Citrate, a critical intermediate in the Krebs cycle, is highly concentrated in native bone (90% of the body's total citrate content is in the skeletal system) and is reported to be closely associated with bone metabolism and formation. Citrate serves as a calcium-solubilizing agent and plays an essential role in the anatomy and physiology of bone apatite nanocrystals [23], which regulate and provide bone with its unique load-bearing properties [24]. Critically, citrate-based composite materials formulated with HA microparticles are extensively reported to promote osteogenic differentiation of hMSCs *in vitro* [25] and osteochondral repair processes in pre-clinical animal models [22,26–28].

In this study, a citrate-based composite, poly(octamethylene citrate) (POC), was synthesized using two acid-to-diol ratios (POC 1:1.1 and POC 1:1.3) and formulated into a resorbable composite material (POC-HA) through the addition of hydroxyapatite microparticles. The mechanical, degradation, and biocompatibility properties of the POC-HA citrate composite materials were assessed relative to a control (PLDLA-TCP) biodegradable composite commonly used in FDA-approved biodegradable orthopedic devices. Furthermore, the potential of these materials in activating hMSC osteo-responsive signaling pathways was assessed *in vitro* via RNA sequencing and computational pathway analysis. Finally, POC-HA composites were fabricated into suture anchors, implanted into a sheep metaphyseal defect model, and assessed *in vivo*.

POC-HA composites were observed to enable cell adhesion, proliferation, and differentiation of hMSCs into an osteogenic lineage, as evidenced by the deposition of calcified extracellular matrix (ECM), production of alkaline phosphatase (ALP), and expression of osteogenic marker osteopontin (OPN). In addition, hMSCs cultured on POC-HA composites underwent an increase in osteoresponsive signaling pathway activation, leading to osteoinduction, osteoconduction, ECM deposition, maturation, and mineralization. Pre-clinical evaluation of POC-HA composites in a sheep metaphyseal model further supported the osteogenic capacity of the POC-HA composite material *in vivo*, and enhanced peri-implant integration was observed relative to a control PLDLA-TCP anchor. Together, this study presents a comprehensive *in vitro* and *in vivo* analysis of a citrate-derived composite tendon anchor and indicates that citrate-based HA composites offer improved mechanical and osteogenic properties relative to resorbable tendon anchor devices formulated from PLDLA-TCP.

2. Results

2.1. Mechanical analysis of POC-HA and control PLDLA-TCP composites

To assess the compressive mechanical properties of the formulated citrate-based composites, uniaxial compressive analysis of POC 1.1-HA, POC 1.3-HA, and control PLDLA-TCP composites was performed under ambient conditions using a strain rate of 1.3 mm/min. POC 1.1-HA and POC 1.3-HA composites demonstrated similar stress-strain responses (Fig. 1a) typical of an elastomeric material exceeding 40 % strain at peak stress. In contrast, the stress-strain responses of the PLDLA-TCP composite showed plastic deformation and underwent less than 10 % strain at peak stress. The compressive modulus (Fig. 1b) of PLDLA-TCP composites was significantly higher than POC-HA composites, with no significant difference between POC 1.1-HA and POC 1.3-HA composites observed. Conversely, the peak stress of both citrate-based composites was significantly higher than PLDLA-TCP. Interestingly, POC 1.1-HA composites showed a slightly higher peak stress and strain (Fig. 1c&d) than POC 1.3-HA, possibly due to increased available carboxylate chemistry for polymer-bioceramic interactions.

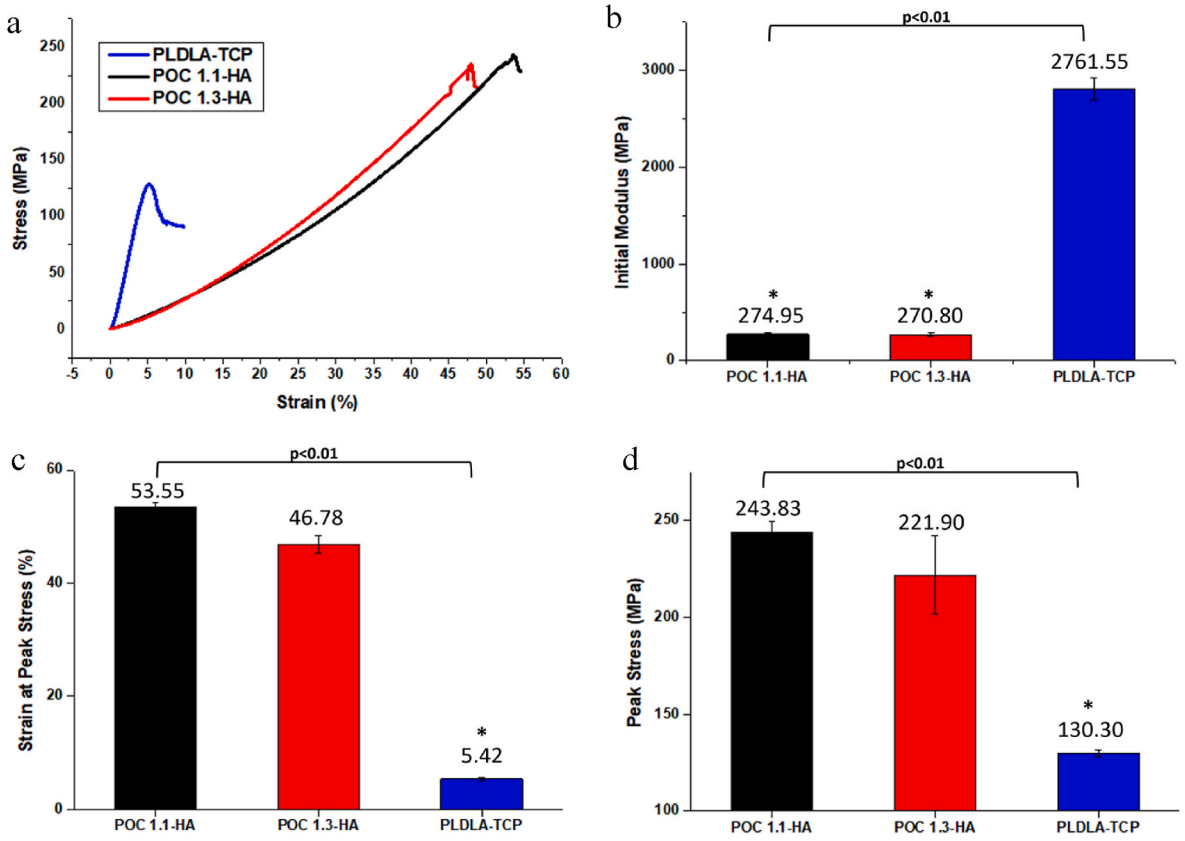

Fig. 1. Uniaxial compression testing of POC-HA and PLDLA-TCP composites A) representative stress-strain curves, B) initial modulus, C) strain at stress, and D) peak stress. Data is represented as mean ± standard deviation. n = 4, * indicates p value of significance <0.01.

2.2. Degradation analysis of POC-HA and control PLDLA-TCP composites

White light interferometry was performed to assess the surface topography of POC 1.1-HA, POC 1.3-HA, and PLDLA-TCP composite materials before and after cell seeding (Fig. 2a). Non-degraded (day 0) PLDLA-TCP composites possessed a heterogenous surface morphology with relatively large pit and peak features resulting in an increased roughness relative to both POC formulations at day 0. PLDLA-TCP composites were observed to undergo surface degradation 7 days post hMSC seeding, as identified through a significant increase in surface arithmetic mean height S_a (Fig. 2b). Conversely, the roughness of POC 1.1-HA and 1.3 POC-HA formulations were not observed to significantly change by day 14 (Fig. 2a and b).

Polymer hydrolysis was conducted under accelerated conditions at 77 °C in phosphate buffered saline (PBS) for POC-HA and PLDLA-TCP composites. PLDLA-TCP composites displayed rapid polymer degradation under these degradation conditions, with complete polymer loss after 20 days. In contrast, POC composites displayed complete polymer hydrolysis after 70 days (Fig. 2c). POC 1.3-HA composites initially resisted polymer hydrolysis when compared to POC 1.1-HA composites due to the enhanced polymer chain crosslinking and reduction in hydrophilic carboxylate groups.

2.3. Differential scanning calorimetry (DSC) of POC-HA and PLDLA-TCP composites

Fig. 3 shows the DSC heat flow curves for POC 1.1-HA, POC 1.3-HA, and control PLDLA-TCP composites at 0, 7, and 14 days post hMSC seeding. The onset of glass transition for POC 1.1-HA materials (Fig. 3a) was observed to occur at −42 °C in non-degraded samples, was shifted to ca.- 21 °C at 7 days post degradation and was not present by 14 days post cell seeding.

The polymer's sizeable leathery region (−41.94 to −0.91 °C) suggested a wide variation of chain molecular weight within the polymer matrix. The shift in the onset of glass transition temperature to −21 °C at 7 days post-cell seeding and the absence of this transition temperature at 14 days post-cell seeding suggested a polymer degradation as a function of molecular weight. A notable endothermic peak at 110 °C progressing above the baseline at ca. 150 °C was observed, suggesting thermal degradation.

POC 1.3-HA composites also demonstrated a similar trend (Fig. 3b); however, this composite demonstrated increased stability relative to POC 1.1-HA, and a glass transition phase was still present at 14 days post-cell seeding. There were no significant changes in the onset of the glass transition temperature or the glass transition region as a function of cell culture duration between the POC 1.1-HA and POC 1.3-HA composites. Conversely, PLDLA-TCP composites demonstrated amorphous behavior and a glass transition temperature of 55 °C (Fig. 3c), which was observed to decrease by day 7, followed by an increase at day 14, suggesting a non-linear degradation process.

2.4. Fourier transform infrared (FTIR) spectroscopy of POC-HA and control PLDLA-TCP composites

FTIR analysis of POC 1.1-HA and POC 1.3-HA composites was performed on non-degraded samples (day 0) and at 7 and 14 days following hMSC seeding to assess cell-mediated degradation of nanocomposite surface chemistry (Fig. 3d). FTIR spectra were characteristic of POC elastomer chemistries and bands were observed at (i) 1728 cm^{-1} (C=O stretching), at 3397 cm^{-1} (assigned as hydrogen-bonded hydroxyl groups) at 1187 cm^{-1} and 1019 cm^{-1}, both assigned to stretching of *C*–O bonds.

Fig. 3d also shows the FTIR spectra of PLDLA-TCP at days 0, 7, and 14 following hMSC seeding. The characteristic polylactide bands of PLDLA were observed at 1033, 1081, and 1267 cm^{-1} (=C–O stretching), 1451 cm^{-1} (CH3 bending), 1747 cm^{-1} (C=O stretching in the ester group), 2918 cm^{-1} (CH stretching) and 2994 cm^{-1} (CH3 stretching). Shifts in polylactide bands at 1033, 1081, and 1267 (=C–O stretching), 1360 and 1381 cm^{-1} (CH2 wagging), 1451 cm^{-1} (CH3 bending), 1747 cm^{-1} (C=O stretching in the ester group) were observed. Previous research suggests these minor shifts are due to a change in microphase domains due to copolymer-solvent interaction. This behavior is also supported by DSC analysis. The shift in wavelength observed on the 7th

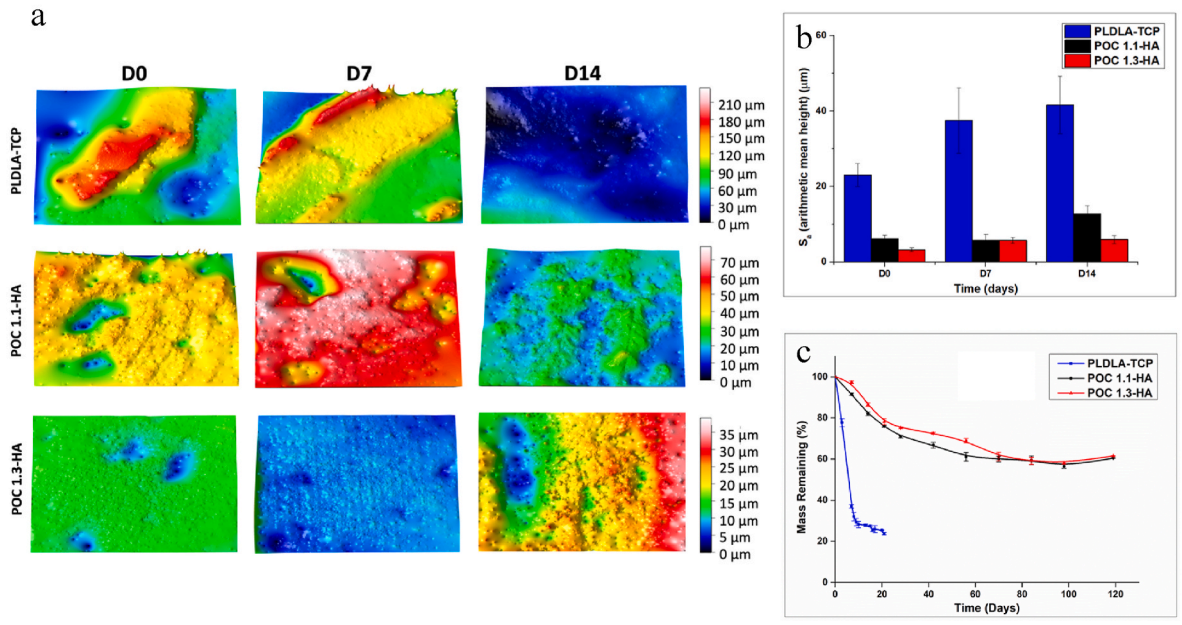

Fig. 2. The effects of *in vitro* degradation on the surface roughness and mass loss of POC 1.1-HA, POC 1.3-HA and PLDLA-TCP substrates *in vitro*. Surface profilometry imaging (a) and subsequent analysis (b) of roughness (S_a) of PLDLA-TCP, POC 1.1-HA and POC 1.3-HA substrates maintained in PBS at for up to 14 days at 37 °C. Accelerated degradation analysis of mass loss of POC 1.1, POC 1.3 and PLDLA-TCP substrates immersed in PBS at 77 °C for up to 120 days (c).

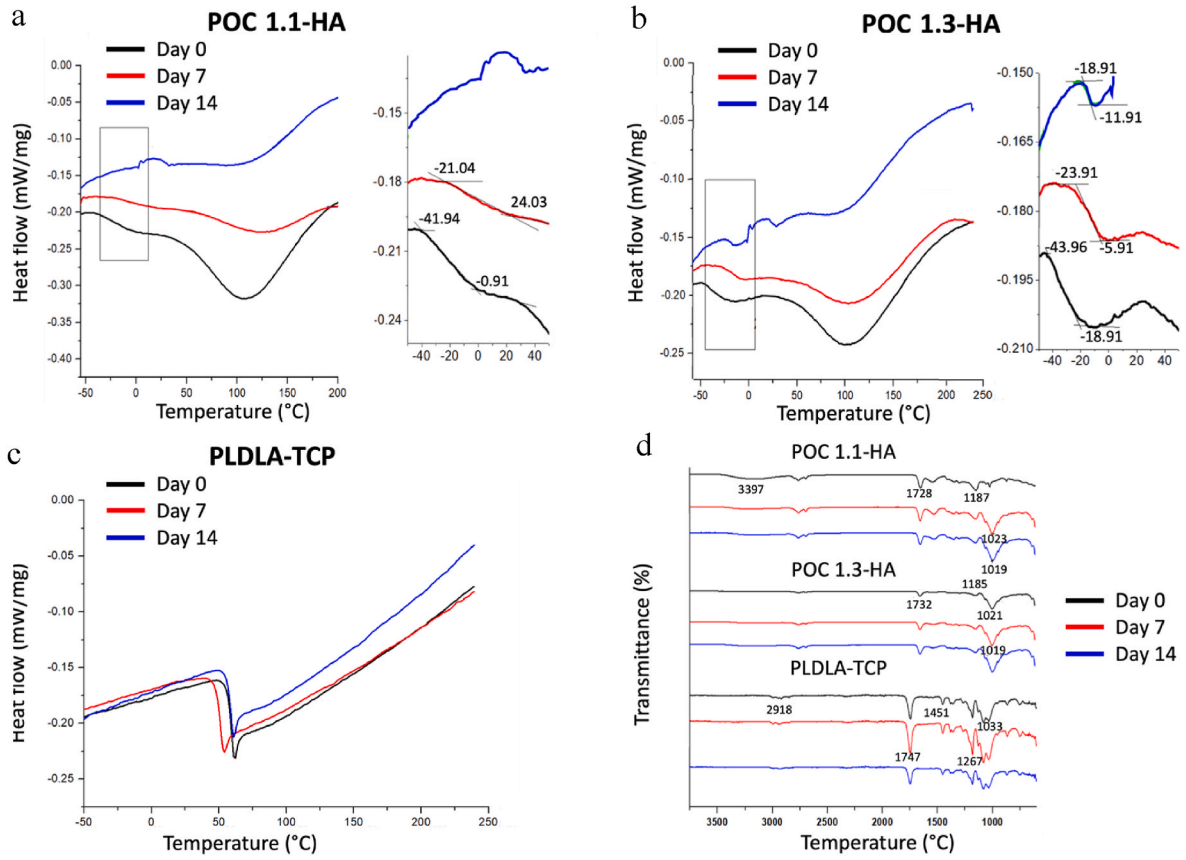

Fig. 3. DSC analysis of POC 1.1-HA, (a) POC 1.3-HA (b), and PLDLA-TCP (c), at 0, 7, and 14 days post-cell seeding. FTIR Spectra of POC 1.1-HA, POC 1.3-HA and PLDLA-TCP control substrates pre-cell seeding (day 0), and on day 7 and day 14 post-cell seeding (d).

day in PLDLA-TCP spectra was again observed at day 14 post-hMSC seeding.

2.5. *In vitro analysis of POC-HA cytocompatibility*

Calcein staining of hMSCs (Fig. 4A a-d) indicated that pristine POC formulations without bioceramic addition did not support cell adhesion and growth. In contrast, POC 1.1-HA, POC 1.3-HA, and PLDLA-TCP composites supported cell adhesion and proliferation for 21 days *in vitro* (Fig. 4a–d). *Alamar blue* assay indicated that hMSCs cultured on POC 1.1-HA and POC 1.3-HA formulations demonstrated a significant decrease in metabolic activity at all time points relative to hMSCs cultured on tissue culture plastic under osteogenic conditions (Fig. 4B). Conversely, hMSCs seeded on the control PLDLA-TCP composite showed a statistically significant increase in metabolic activity at 7 and 14 days relative to both POC-HA formulations. This trend continued until day 28, with respect to the POC 1.1-HA composite (Fig. 4B).

Further metabolic analysis was performed using an Agilent Seahorse XFP cell analyzer to assess the modulation of cellular energy status resulting from mitochondrial respiration in hMSCs exposed to POC-HA and PLDLA-TCP composite conditioned media. Two parameters of cellular energy status, oxygen consumption rate (OCR) (Fig. 4C) and extracellular acidification rate (ECAR) (Fig. 4D), were measured during the assay. While OCR is an essential metric for cellular respiration, recent research has shown that ECAR is significantly modulated by cellular glycolysis and CO_2 produced by the citric acid cycle during respiration [29] as well as by the pentose phosphate pathway, which is crucial for the survival of cancer cells [30]. The oxygen consumption rate was observed to significantly increase in hMSCs cultured on POC 1.3-HA and in hMSCs cultured under osteogenic media on tissue culture plastic relative to hMSCs cultured on POC 1.3-HA and control PLDLA-TCP substrates under baseline and stressed conditions (Fig. 4C). No significant differences were observed in ECAR between the experimental or control groups (Fig. 4D).

2.6. *In vitro assessment of POC-HA osteogenic potential*

The osteogenic differentiation of hMSCs cultured on POC-HA and PLDLA-TCP composites was assessed through the expression of osteogenic marker osteopontin, the quantification of ALP production, and the deposition of mineral calcium under normal and osteogenic culture conditions.

Quantification of gene expression revealed increased OPN production in hMSCs cultured on both POC-HA composites relative to hMSCs cultured on PLDLA-TCP control composites under both normal and osteogenic conditions and at all investigated time points (Fig. 5a). Interestingly, by day 14, OPN expression of hMSCs cultured on POC-HA composites under normal growth media conditions was comparable to OPN expression of hMSCs cultured on control TCP conditions under osteogenic growth conditions (Fig. 5a).

Quantitative analysis of calcium deposition in hMSCs cultured on POC-HA and the PLDLA-TCP composites in osteogenic induction media and normal hMSC growth media for 7, 14, and 21 days indicated a time-dependent increase in calcium deposition on both POC-HA composites relative to cells cultured on the control PLDLA-TCP composite (Fig. 5b). hMSCs cultured on POC 1.1-HA and POC 1.3-HA composites under osteogenic induction and normal growth media showed increased calcium deposition relative to PLDLA-TCP control composite materials at days 14 and 21. Critically, by day 14 and 21, hMSCs cultured on POC 1.3-HA composites in normal growth medium demonstrated greater calcium deposition than cells cultured in osteogenic induction media. hMSCs cultured on control PLDLA-TCP composites demonstrated no

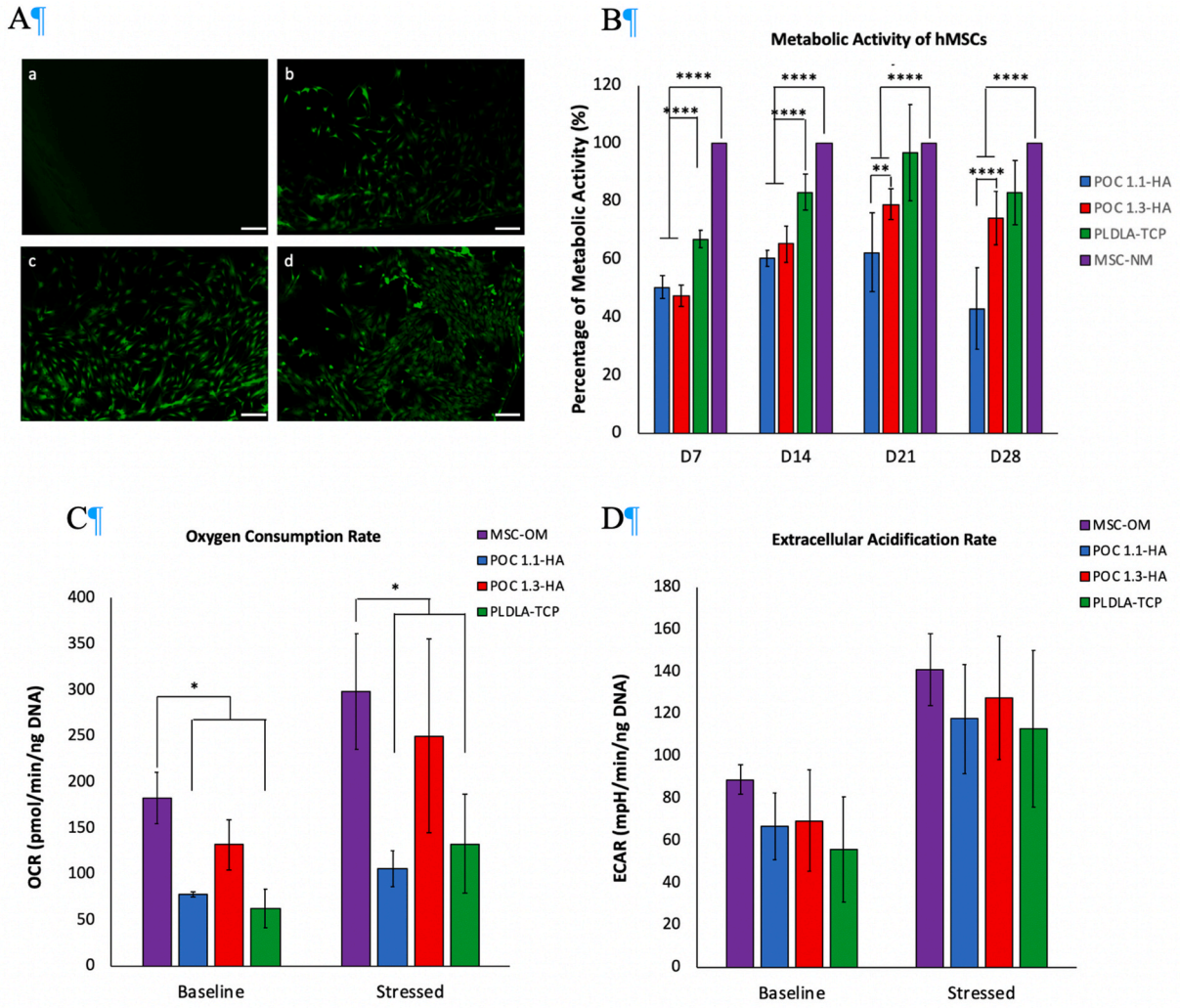

Fig. 4. Representative images of Calcein staining showing adhesion and growth of hMSCs on POC (a), POC 1.1-HA, (b), POC 1.3-HA (c) and PLDA-TCP (d). Scale bar 200 μm. Metabolic activity of hMSCs cultured on POC-HAs, PLDLA and tissue culture plastic for 7, 14 and 21 days normalized to cells in tissue culture plastic (B). hMSCs cultured on POC 1:1.3 composites demonstrated increased oxygen consumption rate relative to POC 1:1.1 and PLDLA-TCP control substrates (C). No significant differences in extracellular acidification rate were observed between any of the experimental or control groups (h). n = 3.

significant difference in calcium deposition between osteogenic and normal media conditions at any time point but a relative decrease in calcium deposition over time. Conversely, hMSCs cultured on tissue culture plastic significantly increased calcium deposition when cultured under osteogenic induction media at all time points.

Similarly, ALP synthesis was significantly greater in hMSCs cultured on POC 1.3-HA composites than in hMSCs cultured on PLDLA-TCP control composites and tissue culture plastic controls under normal growth media and osteogenic growth media conditions. Interestingly, hMSCs cultured on all experimental and control composite materials in normal and osteogenic growth media demonstrated a significant increase in ALP production relative to cells cultured on control tissue culture plastic (Fig. 5d) [26,31].

2.7. Transcriptomics profiling of hMSCs cultured on citrate-based composites

To assess the modulation of hMSCs signaling pathways on citrate-based composites, transcriptomics profiling of hMSCs cultured for 7, 14, and 21 days was carried out by stranded transcriptome mRNA sequencing. Transcript counts were used to calculate differentially expressed genes (DEG) for POC 1.1-HA and POC 1.3-HA, a positive control of hMSCs cultured in osteogenic growth media on tissue culture plastic and a gold standard control of a PLDLA-TCP composite. Analysis was performed at each time point using DESeq2 relative to hMSCs cultured in normal growth media on tissue culture plastic. Principle component analysis (PCA) of all samples revealed a distinct separation between undifferentiated hMSCs cultured on control tissue culture plastic substrates and hMSCs cultured on experimental and control composite materials (Fig. 6a). The number and distribution of differentially expressed genes at each time point are detailed in Fig. 6b and c, respectively.

2.7.1. Osteo-specific function analysis

To assess the effects of the investigated composites on osteospecific signaling pathways and bio functions, canonical pathways leading to osteoinduction, osteoconduction, growth factor binding, cellular remodeling, and cellular metabolism, along with enriched functions related to the extracellular matrix, hMSC differentiation, cell attachment, angiogenesis, and vasculogenesis were explored for each composite at day 7, 14 and 21 (Table S1). Critically, the modulation of canonical osteospecific signaling in hMSC populations cultured on POC 1.1-HA, POC 1.3-HA, and control PLDLA-TCP composites at each time point was assessed in detail, and activated pathways were classified according to specific osteo-responsive roles, specifically osteoinduction, osteoconduction, growth factor signaling, and cellular metabolic

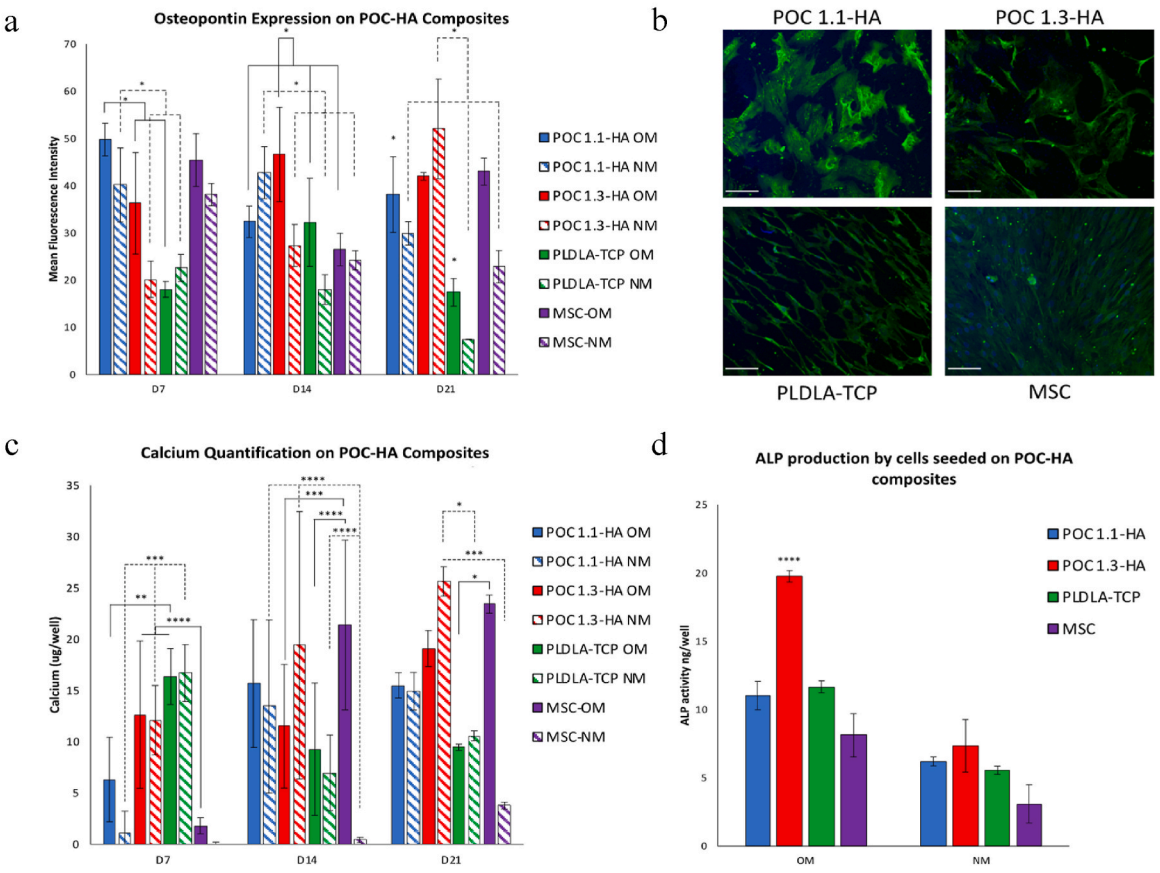

Fig. 5. The *in vitro* osteospecific response of hMSCs cultured on POC-HA composites. Quantification of osteopontin expression (a) and immunostaining of osteopontin expression (b) in hMSC cultured on POC-HA and PLDLA-TCP composites in normal growth medium (NM) at day 21. Green osteocalcin, blue nucleus. (Magnification 20 ×, sale bar 100 μm. Calcium deposition (c) of hMSCs cultured on POC-HA and PLDLA-TCP composites in either osteogenic induction media (OM) or normal growth medium (NM) for 7, 14 and 21 days. Quantification of ALP activity measured on day 14 h in hMSCs cultured in OM (d).

pathways (Fig. 7a).

RNA-Seq analysis indicated transcriptional changes in the genes associated with the enrichment of bone morphogenetic protein (BMP), ERK/MAPK, p38 MAPK, RhoGDI, RANK, Wnt/β-catenin, RhoGDI, and JAK/Stat signaling, pathways attributed to osteoinduction. Specifically, multiple pathways associated with osteoinduction were enriched in hMSCs cultured on POC 1.3-HA and control PLDLA-TCP composites relative to cells cultured on TCP controls under normal growth conditions.

Osteoconductive pathway enrichment was observed in signaling processes concerned with cell adhesion and migration, such as Inhibition of MMPs, Actin Cytoskeleton, Integrin, and Paxillin signaling. Similarly, by day 21, most of the enriched pathways associated with osteoconductive processes were upregulated in hMSCs cultured on POC 1.3-HA and control PLDLA-TCP composites relative to cells cultured on TCP controls under normal growth conditions.

Although leading to osteoinduction, growth factor signaling pathways were classified separately, and signaling pathways IGF-1, PDGF, TGF-β, VEGF, and FGF were found to be enriched. Again, by day 21, most enriched pathways associated with growth factor signaling were upregulated in hMSCs cultured on POC 1.3-HA and control PLDLA-TCP composites relative to cells cultured on hMSC controls under normal growth conditions.

Metabolic pathways were of interest because cells undergoing differentiation often require a high energy status to fuel the differentiation process, often marked by increased levels of metabolic activity and activation of metabolic pathways. Enrichment was observed in mTOR, calcium, and AMPK signaling pathways, which were significantly upregulated in hMSCs cultured on POC 1.3-HA and control PLDLA-TCP composites.

2.7.2. *Disease and functions analysis*

Bio-functions leading to ECM changes, hMSC lineage commitment to osteoblasts and chondrocytes, ossification, differentiation of chondrocytes and osteoblasts, neoangiogenesis, sprouting angiogenesis, angiogenesis of bone, vasculogenesis, and inflammatory response were explored in hMSCs cultured on composite and control substrates for up to 21 days *in vitro* via stranded transcriptome mRNA sequencing followed by pathway analysis. The number of genes involved in the dataset corresponding to the above-listed bio functions and their activation state are given in Supplementary Table 1. Enriched bio functions were classified based on their target location and cellular/physiological activity.

The explored enrichment terms were related to ECM formation, binding, mineralization, calcification, and remodeling. hMSC lineage commitment-related terms explored were adhesion, adipogenesis, chondrogenesis, osteoblast differentiation, osteogenesis, mineralization, proliferation, and differentiation. Enriched bio-functions relating to osteogenesis, endochondral ossification, ossification of bone, neoangiogenesis, sprouting angiogenesis, and vasculogenesis were also detected (Fig. 7b).

A comparison of bio-function activation patterns revealed that hMSCs cultured on tissue culture plastic in osteogenic growth media (TCO) demonstrated the greatest number of activated bio-functions at all explored time points. On day 7, hMSCs cultured on PLDLA-TCP showed the highest activation of ECM calcification, hMSC osteogenesis, and hMSC transdifferentiation. Conversely, hMSCs cultured on

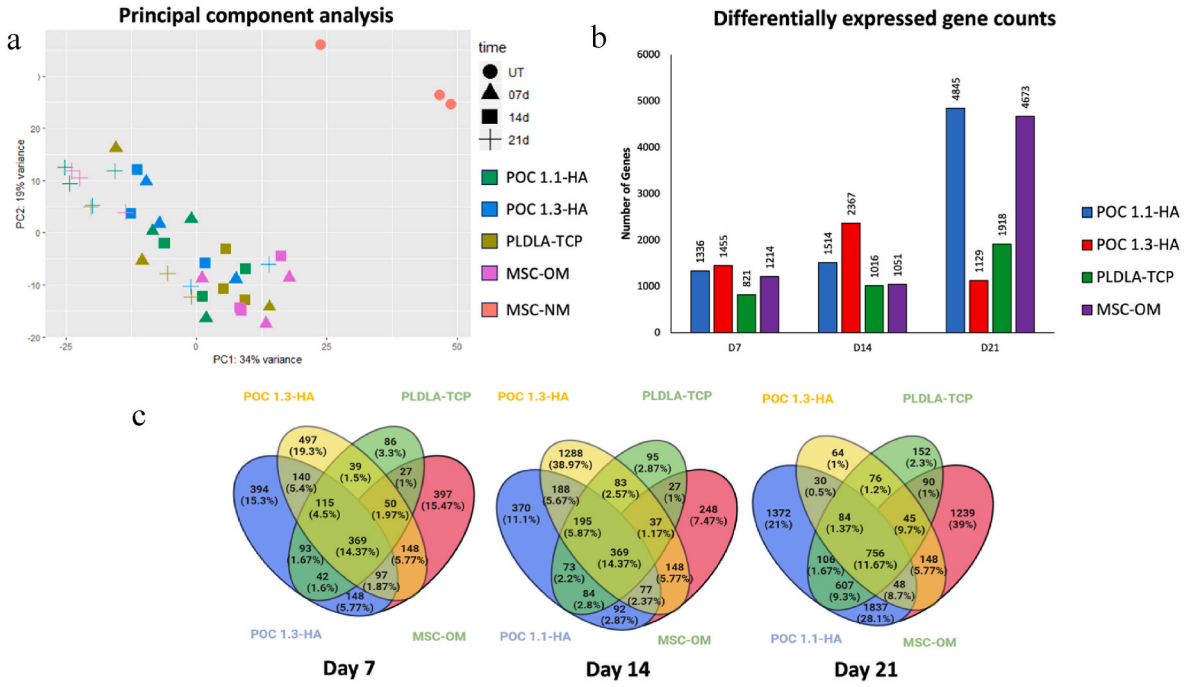

Fig. 6. Principle component analysis (PCA) plot for POC 1.1-HA, POC 1.3-HA, and PLDLA-TCP composites showing a clear separation between undifferentiated hMSCs grown in tissue culture plastic (MSC-NM), undifferentiated hMSCs grown on citrate-based composites and osteogenic differentiated hMSCs grown on tissue culture plastic (MSC-OM) (a). The number of differentially expressed genes for each group at each timepoint (b). Venn diagram showing unique and shared differentially expressed genes for all the composites at day 7 day 14 and day 21 (c). Ingenuity pathway analysis (IPA) was used to interpret differentially expressed genes biologically, generating a list of canonical pathways, diseases, functions, upstream regulators, and mechanistic networks. Pathways with a z score of more than 1.5 were considered significantly activated, while pathways with a z score of less than −1.5 were considered significantly inhibited. Detected enriched gene functions were plotted based on the significance of gene enrichment (-log P-value).

POC-HA composites showed the highest activation of cytoskeletal morphology, cell viability, ECM degradation, and osteogenesis.

On day 14, hMSCs cultured on the control PLDLA-TCP composite exhibited activation of one bio-function (hMSC adhesion). In contrast, hMSCs cultured on POC-HA composites showed the highest activation of 5 (cytoskeletal morphology, sprouting angiogenesis, ECM degradation, osteogenic differentiation of hMSCs, and osteogenesis) and 2 (cell viability and formation of cytoskeleton) bio-functions.

On day 21, hMSCs cultured under TCO conditions showed the highest activation of 19 bio functions. hMSCs cultured on control PLDLA-TCP substrates demonstrated the highest activation of three bio functions (Angiogenesis of bone, hMSC adhesion, and ECM remodeling). In comparison, hMSCs cultured on POC-HA composites showed the highest activation in 4 bio functions (morphology of cytoskeleton, ECM formation, ECM degradation, and hMSC Mineralization). hMSCs cultured on POC-HA composites at day 21 showed the highest activation in 8 bio functions (osteogenesis, ossification, Osteogenesis of hMSCs, hMSC proliferation, hMSC differentiation, ECM binding, ECM deposition, and organization of cytoskeleton). TCO hMSCs at 21 days showed the highest activation in 19 bio-functions.

2.7.3. Gene set enrichment analysis (GSEA)

Gene set enrichment analysis was performed using a Web-based gene set analysis toolkit (webgestalt). Enriched functions were plotted based on their Normalized Enrichment Score (NES) with a 5 % FDR cutoff. Volcano plots of all Enriched biological processes, cellular components, and molecular functions detected for each composite are listed in Supplementary Fig. 1. Furthermore, the effects of citrate-based composites on the temporal and spatial activation patterns of Osteospecific canonical pathways signaling pathways in hMSC populations are given in Supplementary Table 2.

2.8. In vivo metaphyseal implantation study

2.8.1. Histology and microCT analysis

To assess the biocompatibility and integration of citrate composites *in vivo*, bone anchor devices were fabricated from the POC 1.1-HA formulation and implanted into the femur and tibia metaphyseal region in a sheep model. It should be noted that this formulation was selected due to its improved processability relative to the POC 1.3-HA formulation. A schematic of the bone screw and the implantation locations can be found in Supplementary Figs. 2 and 3, respectively. The ratio of the drilled-generated defect area to the screw area was assessed via sequential uCT imaging of both control PLDLA-TCP anchors and POC 1.1-HA anchors at 3 and 6 months post-implantation and of POC 1.1-HA anchors at 12 and 36 months post-implantation (Fig. 8a). Two-way ANOVA revealed a significant difference ($p = 0.025$) regarding the effect of time but not the biomaterial formulation on anchor integration. Bone anchor integration underwent a statistically significant increase at 36 months post-implantation with a ratio of 75.9 ± 7.63 % versus the 3-month time point with a ratio of 60.39 ± 3.74 % ($p = 0.011$) (Fig. 8b and c). Histopathological analysis of bone tissue indicated that at 12 months post-implantation, some tendon tissue was replaced with trabecular calcified bone tissue at the peri-implant region. This observation was further realized 36 months post-implantation (Fig. 8d). Supplementary Fig. 5 shows the determination of tissue area through histomorphometric analysis.

2.8.2. Biomechanical analysis

All biomechanical tests were run to completion. The ultimate load before tendon failure is expressed in Fig. 8e. No significant differences in the ultimate load were observed between the POC 1.1-HA and PLDLA-TCP groups. The mode of failure (tendon-bone interface, tendon midpoint, or tendon-clamp interface) is detailed in Supplementary Table 3.

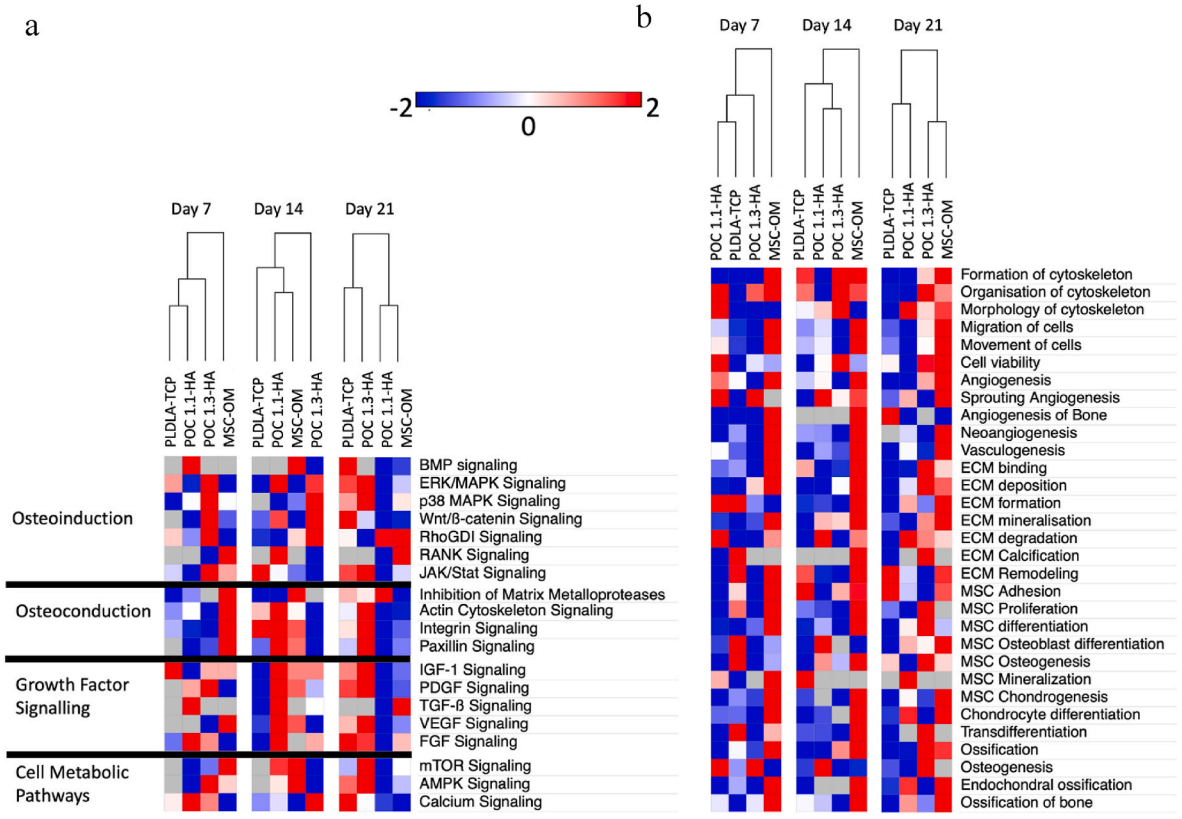

Fig. 7. Analysis of the functional response of hMSCs to citrate composite materials. Heat map of osteo-responsive signaling pathways activated by POC 1.1-HA, POC 1.3-HA, and PLDLA-TCP (a) and heat map of enriched Bio-functions (b) leading to cytoskeletal rearrangement, cell migration, viability, blood vessel formation, extracellular matrix related functions, hMSC functions and lineage commitment and ossification related terms activated by citrate-based polymer composites (POC 1.1 and POC 1.3), and cells cultured on control PLDLA-TCP and tissue culture plastic substrates under osteogenic conditions. Plot based on activation score (Z value). A positive Z value represents activation of the biological function, while a negative Z value represents inhibition of the function. Analysis was performed relative to hMSCs cultured on tissue culture plastic under normal growth media conditions.

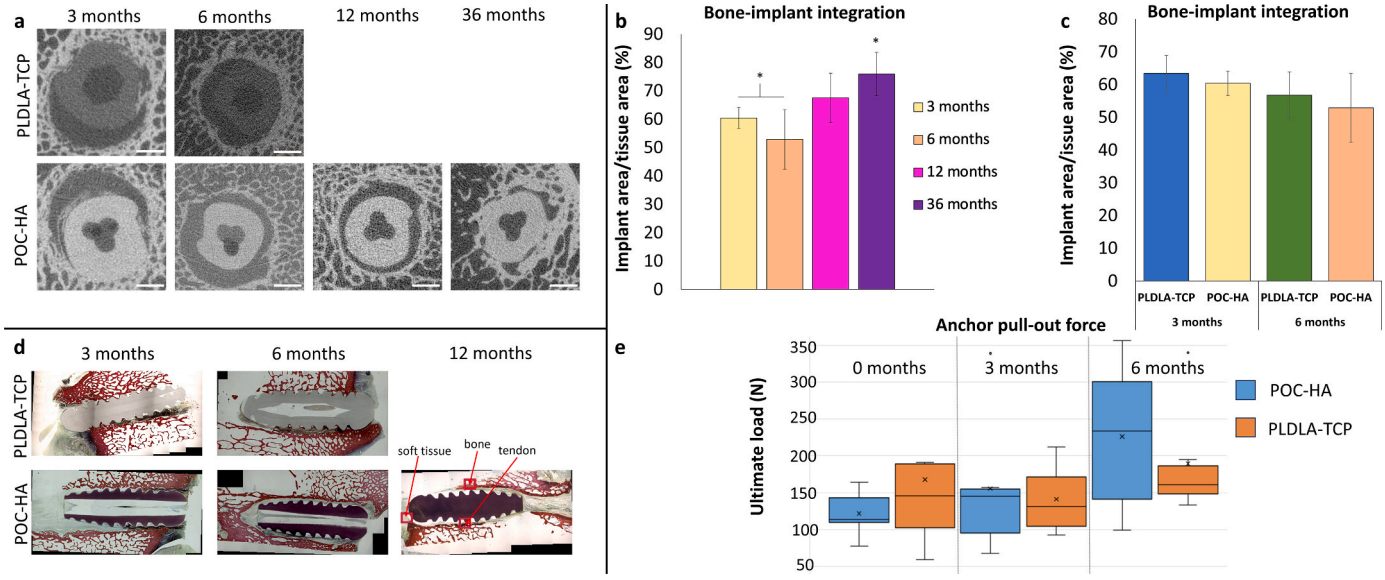

Fig. 8. MicroCT and histological analysis of POC-HA and PLDLA-TCP bone anchor implants. MicroCT images depict the implant inside the tissue cavity, scale bar: 2 mm (a). Quantification of peri-implant tissue integration. significant reduction in peri-implant void was observed at 36 months post-implantation of citrate-HA tendon anchor devices (b), however, no significant differences were observed between groups at 6 months post-implantation (c). Histological analysis of the peri-implant region at 12 months post-implantation revealed that the presence of soft tissue was reduced and replaced by bone tissue (d). Ultimate load of Acuitive and Control treatments at the three time points. The "box" is bounded by the first and third quartiles; the "whiskers" represent the maximum/minimum values within the data set; the median data bar, mean data 'x', and outliers '·' are highlighted. There were no significant differences between treatments ($p = 0.910$), timepoints ($p = 0.100$), or treatment-timepoint interactions ($p = 0.710$). Statistical significance of $p < 0.05$ is indicated *.

3. Discussion

Citrate, an intermediator of the tricarboxylic acid cycle, drives the oxidation of multiple nutrients to produce chemical energy in the form of ATP. As well as playing a pivotal role in eukaryote metabolism, the abundance of citrate in bone was first observed by Dickens et al. in 1941 [32], who showed that ~90 % of the body's citrate is localized within mineralized tissues and makes up ~1.6 % of the bone content. Incorporating citrate imparts significant biomechanical properties to the bone, enhancing tissue strength and resistance to fracture. Even though the role of citrate in bone apatite crystal stabilization and bone mineralization has been known for several decades, few studies have confirmed the biocompatibility and osteomimetic properties of citrate-derived biomaterials and the ability of citrate to increase cell metabolism *in vitro* [33–35].

In this study, citrate-based thermoset composites formulated with two different acid-to-diol ratios (POC 1.1-HA and POC 1.3-HA) were synthesized and initially assessed with respect to surface chemistry, degradation rate, and polymer bioceramic interaction. These two citrate-based HA composites were further explored as orthopedic biomaterials, and their ability to induce osteospecific processes *in vitro* and bone remodeling *in vivo* was compared to that of the thermoplastic composite (PLDLA-TCP), widely used in FDA-approved biodegradable orthopedic devices.

Physicochemical analysis revealed that POC composites underwent polymer hydrolysis at a significantly slower rate than PLDLA-TCP composite materials, which were observed to undergo a non-linear degradation process by DSC analysis. This accelerated degradation of PLDLA-TCP composites relative to POC-HA materials was also indicated by an increased surface roughness following a 7-day cell culture study.

Previous studies have reported that citrate-based HA polymer blends and bio-resorbable polymer composites employing a microscale mineral phase enhanced osteoinductivity and osteoconductivity [14–17], improved surface adhesion of osteoblasts [20], evoked long-term bone and cartilage responses [21,22] and increased the expression of ALP and osterix [18] *in vitro* and *in vivo*. In this study, cytocompatibility analysis of the *in vitro* response of hMSC populations to POC-HA and control PLDLA-TCP materials indicated that cells cultured on PLDLA-TCP composites showed a statistically significant increase in metabolic activity at 7 and 14 days relative to both POC-HA formulations. Conversely, POC 1.3-HA formulations were observed to induce increased expression of ALP, osteopontin, and calcium deposition in hMSC populations relative to POC 1.1-HA and control PLDLA-TCP composites.

Transcriptomics profiling by RNA Sequencing has emerged as a powerful tool to elucidate molecular mechanisms underlying biological functions in a cell population. Herein, we profiled transcriptomics changes in hMSCs cultured on POC-HA and control PLDLA-TCP composites using RNAseq and subsequent bioinformatics Ingenuity pathway analysis (IPA). IPA analysis revealed that the hMSC population cultured on POC 1.1-HA and POC 1.3-HA composites demonstrated increased activation of multiple signaling pathways and enriched hMSC biological and cellular functions beneficial for osteochondral regeneration and repair.

Transcriptomics analysis of hMSCs cultured on POC-HA composites revealed activation of canonical pathways and enriched molecular/cellular functions relating to osteoinduction and osteoconduction. POC 1.3-HA, in particular, was the most osteoresponsive polymer composite, activating 35 (46.6 %) of all osteo-responsive pathways detected. Cells alone in osteogenic media and cultured on POC 1.1-HA and PLDLA-TCP composites positively activated 37.3 %, 36 %, and 28 % of all osteo-responsive pathways detected, respectively.

Several enriched ontology functions were also detected. These included osteogenesis, ossification, ECM deposition, ECM mineralization, and tissue angiogenesis. Interestingly, significant upregulations in pathways associated with the mineralization of tendon tissues were observed, indicating that citrate materials may be beneficial in fabricating tendon anchor devices.

A pilot animal study was conducted to assess the efficacy of a single POC-HA formulation (POC 1.1-HA) on tendon anchoring and peri-implant osteoneogenesis. Due to challenges with manufacturing, this was the only POC formulation examined in this study. Although no significant differences in peri-implant bone regeneration were observed between POC and the control PLDLA-TCP group, a significant increase in peri-implant bone formation was observed with the POC anchor following 12 and 36 months *in situ* relative to the 3-month time-point. Further biomechanical analysis indicated no significant differences in anchor pull-out forces were observable at 6 months post-implantation, which agrees with the peri-implant bone deposition data. However, a significant limitation of the animal study was the need for a control group post 6 months of implantation, which frustrates the ability to draw definitive conclusions about the long-term functionality of citrate-HA tendon anchors *in vivo*. It is encouraging, however, that citrate-based polymer tendon anchors performed at least as well as control clinically available PLDLA-TCP devices *in vivo* for up to at least 6 months post-implantation. Further studies will evaluate the *in vivo* functionality of POC-derived anchors fabricated from the more promising POC 1.3-HA formulation.

In conclusion, this study provides evidence of the osteogenic potential of POC-HA composites and indicates that citrate-based composite materials possess the potential for osteointegration and osteoinduction relative to the industry standard resorbable material PLDLA-TCP.

4. Experimental section

4.1. Materials

Fully characterized human bone marrow-derived mesenchymal stem cells (hMSCs) from three healthy donors were obtained from collaborating researchers at the National University of Ireland, Galway. Bone marrow aspirations were performed at the Translational Research Facility at University Hospital Galway following institutional ethical committee guidelines. Cell culture media and supplements were purchased from Gibco unless stated otherwise. All general chemicals, reagents, FBS, and osteogenic induction media components were purchased from Sigma Aldrich unless stated otherwise. All primary antibodies used in the study were purchased from Abcam. Secondary antibodies and Alamar blue used in the study were purchased from Thermo Fischer. Calcein stain was purchased from Invitrogen. A calcium quantification kit was purchased from Stanbio. For ALP quantification, a 1-step PNPP substrate was purchased from Sigma Aldrich. For RNA isolation, homogenization columns and isolation kits were purchased from Qiagen. Bioanalyzer chips and reagents were purchased from Agilent. PCR primers were purchased from IDT. Polymerases and other molecular biology reagents were purchased from Promega. Lo bind RNA microcentrifuge tubes were purchased from Eppendorf.

4.2. Cell culture

hMSCs were culture expanded in MEM-alpha medium + GlutaMax (Gibco) supplemented with 10 % FBS (Sigma Aldrich) and 1 % Penicillin streptomycin (Gibco). For osteogenic induction, DMEM low glucose (Sigma Aldrich) supplemented with 100 nM dexamethasone, 100 μm ascorbic acid 2 phosphate, 10 mM Beta glycerophosphate, 10 % FBS and 1 % penicillin-streptomycin. All experiments were performed in biological and technical triplicates.

4.3. Preparation of citrate-based composites

Citrate-based composites were synthesized as previously reported [36]. Briefly, during the pre-polymer synthesis, citric acid (Fisher) and 1,8-octanediol (Sigma) were reacted together in a 1:1.1 acid-to-diol ratio

(POC 1.1-HA) or a 1:1.3 acid-to-diol ratio (POC 1.3-HA) at 140 °C until the desired viscosity was obtained. The pre-polymer was dissolved in ethanol (Fisher) and composited with hydroxyapatite (Sigma) (60 wt.-%) (POC 1.1-HA or POC 1.3-HA). The composite was mixed until homogeneous, molded into the desired sample shape, and crosslinked at 80 °C for 7d.

4.4. Preparation of PLDLA composites

PLDLA 70/30 (Corbion) was dissolved in dichloromethane (Fisher) and composited with 15 wt.-% tricalcium phosphate (CaP Biomaterials) (PLDLA-TCP). After mixing until homogeneous, the resulting composite was molded into a disk shape.

4.5. Compressive mechanical properties

Unconfined compression tests were performed using an Electromechanical Universal testing machine Q Test-150 (MTS, Eden Prairie, MN, USA) to evaluate the compressive mechanical properties. Briefly, cylindrical-shaped specimens 6 × 12 mm^2 (diameter x height) were compressed at a rate of 1.3 mm/min to failure. The initial modulus was calculated by measuring the gradient at 10 % of compression of the stress–strain curve. The results are presented as mean±standard deviation (n = 4).

4.6. Composite degradation

The degradation rate of the 6 × 12 mm^2 (diameter x thickness) cylindrical samples was assessed *in vitro* in phosphate buffered saline (PBS) (pH 7.4) at 77 °C under static conditions. PBS was changed weekly to ensure the pH did not drop below 7. Samples were extensively rinsed with deionized water and lyophilized at predetermined time points before weighing. Weight loss was calculated by comparing the initial weight (W_0) with the weight measured at predetermined time points (W_t), as shown in Eq. (1). The results are presented as mean±standard deviation (n = 6).

Equation 1:

$$\text{Mass loss} = (W_0 - W_t)/W_0 * 100\% \quad (1)$$

4.7. Analysis of surface topography and roughness

Surface roughness variations were tested using white light interferometry via a Filmetrics Profilm 3D non-contact profilometer (20 × objective lens used with a 4 × optical zoom). The PLDLA-TCP, POC 1.1-HA, and POC 1.3-HA substrates were immersed in 1x phosphate buffer saline (PBS) for up to 14 days (D14), six images were collected for each condition, and both the average arithmetic mean deviation (Ra) and maximum height (Rz) were recorded in the line roughness (1D) mode. To get an overview of the 2D profile, the arithmetic mean height (Sa) and root mean square height (Sq) were recorded via the area roughness method. Based on these measurements, the surface topography and the roughness variation in both 1D and 2D were analyzed.

4.8. Cell seeding

hMSCs were seeded on biomaterial samples to assess their viability, metabolic activity, and osteogenic differentiation capacity. Tissue culture plastic was used as a control. The samples were washed in 70 % ethanol and soaked overnight in hMSC growth medium in a CO_2 incubator before cell seeding. hMSCs were seeded at the desired plating density in a volume not exceeding 150 μL. The cell-seeded samples were allowed to stand for 1hr in a CO_2 incubator at 37 °C to initiate cell attachment. The samples were then transferred to a 12-well tissue culture plate and carefully supplemented with 3 mL growth medium per well. The growth medium was replaced every three days.

4.9. Calcein staining for assessment of cell attachment

hMSCs were seeded at a density of 1 × 10^5 cells/cm^2 per sample in a 12-well tissue culture plate, as explained previously. The cells were cultured in complete hMSC growth medium for 7 days before staining for calcein. The working dilution of the calcein stain was produced per the manufacturer's instructions. The media was aspirated and 750 μL of working dilution of calcein stain was added on top of the composite surface and incubated for 30 min in a CO_2 incubator at 37 °C. The cells were subsequently viewed under an inverted fluorescent microscope (Olympus), and cell attachment was documented in brightfield and FITC channels.

4.10. Alamar blue metabolic activity assay

The metabolic activity of hMSCs was assessed using the Alamar blue assay. hMSCs were seeded on circular discs of POC (without HA, which resulted in negative values and thus was removed from the graph), POC 1.1-HA, POC 1.3-HA, PLDLA-TCP composites, and on tissue culture plastic treated with normal media as described previously. Briefly, 1 × 10^5 cells were seeded per sample and cultured for 7, 14, 21, and 28 days in hMSC growth medium to assess the metabolic activity of cells. At the end of each time point, the media was aspirated, the sample was washed in sterile PBS, and 1 ml of Alamar blue reagent (1/10 dilution in complete hMSC media) was added to each sample and incubated in a CO_2 incubator for 5hr at 37 °C. After incubation, the supernatant was collected and transferred to 96 well black plates (200 μl/well), and the fluorescence was measured at 570 nm. Alamar blue reagent added to wells without composite or hMSCs served as the negative control, while hMSCs grown in tissue culture plastic (no polymer) served as the positive control. Each composite's percentage of metabolic activity was expressed at the respective time points normalized to cells on tissue culture plastic.

4.11. Cell energy phenotype assay; seahorse analyzer

The OCR and ECAR of hMSCs were measured using the Seahorse Cell Mito Stress Test with the extracellular flux Seahorse XFp analyzer (Agilent) to assess mitochondrial respiration and glycolysis, respectively [37, 38]. Briefly, hMSCs were seeded in PLL-coated Seahorse XF cell culture plates (25,000 cells per well). As per the manufacturer's instructions, 1 h before flux analysis, samples were placed at 37 °C in a non-CO2 incubator, and the media was replaced by Seahorse Base XF medium supplemented with 1 mm sodium pyruvate, 2 mm L-glutamine, and 10 mm glucose at pH 7.4 for CO_2 and O_2equilibration. During this preincubation, the four drugs necessary to perform the Cell Mito Stress Test were loaded into the XF Sensor Cartridges with a preoptimized concentration of 2 μm for the oligomycin, 1 μm of rotenone and antimycin A (provided already mixed by the manufacturer to be loaded and injected together) and 3 μm of carbonyl cyanide-4 (trifluoromethoxy) phenylhydrazone. All the OCR and ECAR values were normalized by DNA content measured for each well using the Quant-iT PicoGreen dsDNA Assay Kit (Invitrogen, Dublin, Ireland) as previously described [39].

4.12. Osteogenic differentiation of hMSCs cultured on citrate polymers

hMSC osteogenic differentiation potential was assessed by seeding hMSCs supplemented with either osteogenic induction media or normal hMSC growth media. Briefly, 20,000 cells were seeded on samples in a 12-well tissue culture plate as described above. The cells were cultured for 24 h on the composite to allow attachment before changing the medium to Osteogenic induction media or Normal hMSC growth

medium. The cultures were maintained for 7, 14, and 21 days, with media replacement every 3 days. Cells cultured on tissue culture plastic served as a control.

Osteogenic differentiation of hMSCs cultured with and without the addition of osteogenic induction media was assessed by staining calcium deposition with alizarin red and by quantifying calcium deposition and ALP production.

4.13. ALP quantification

ALP activity on cells cultured on citrate-based composites was assessed at 14 days using PNPP assay for ALP quantification. Briefly, the media was aspirated, and cells were lysed and scraped off from the polymer using 50ul of 0.2 % Triton ×100 in 100 mM PBS for 10 min. The lysates were transferred to a microcentrifuge tube. In a 96-well plate, 10ul of lysate per well was added. The PNPP substrate was equilibrated to room temperature in each well, and 100uL of 1-step PNPP substrate was added and mixed well by gentle agitation. The plate was incubated for 30 min at room temperature and protected from light. The reaction was arrested by adding 50 μL, 2 N NaOH per well. The absorbance was measured immediately at 405 nm.

4.14. Calcium quantification

hMSC calcium deposition was assessed using staining for calcium deposition using alizarin red and by quantifying the deposited calcium. The media was removed carefully, and samples were rinsed in PBS thrice. Cells were scraped from the sample surface using 0.5 M HCl, and the contents were transferred to a microcentrifuge tube. The solution was incubated overnight at 4 °C in an incubator shaker, centrifuged to remove any debris, and total calcium was assessed using a Stanbio calcium quantification kit following the manufacturer's instructions.

4.15. Immunocytochemistry for osteogenic markers

hMSCs were stained for osteopontin (OPN) and osteocalcin (OCN) expression. Briefly, hMSCs were seeded at a density of 20,000 cells/cm^2 on each sample using either osteogenic induction medium or normal hMSC medium for 7, 14, and 21 days. Tissue culture plastic was used as a control. Media was replaced every 3–4 days. At the end of each time point, the samples were carefully removed and washed with sterile PBS, and cells were fixed in ice-cold methanol for 20 min at −20 °C. The samples were blocked for 1 h at room temperature in a blocking buffer containing 1 % BSA, 22.5 mg/ml glycine in PBST (PBS+ 0.5 % Tween 20). Primary antibodies for OPN and OCN were added at the desired dilutions. Both osteopontin and osteocalcin antibodies were used at a final concentration of 10 μg/ml dilution (1/200 for OCN, 1/100 for OPN) in a blocking buffer and incubated overnight at 4 °C in a humidified chamber. Negative control samples were incubated with a blocking buffer instead of the primary antibody. Following overnight incubation, the primary antibody was removed carefully, the samples were washed thrice in PBS, and the secondary antibody was added (1/500 dilution) and incubated at room temperature for 1 h, protected from light.

The samples were fixed onto a glass slide, with the side of cell growth facing away from the glass slide. The side of cell growth side is mounted with a coverslip using fluoroshield with DAPI that stains the cell nucleus blue. The slides were allowed to dry overnight in the dark and imaged using a confocal microscope (Olympus Fluoview F1000 system). Images were recorded as z stacks of 1um thickness. Quantification of osteopontin and osteocalcin staining was performed using Image J software.

4.16. Transcriptional profiling of hMSCs

hMSCs from three healthy donors were used in this study in technical triplicates for each polymer and each time point. 2×10^4 cells were seeded on each sample and cultured in normal hMSC media for 7, 14, and 21 days. hMSCs cultured in tissue culture plastic that received osteogenic induction media served as the positive control. hMSCs grown in standard hMSC culture media served as the baseline control.

4.17. RNA isolation and integrity check

Total RNA was isolated from hMSCs cultured on days 7, 14, and 21 using the Qiagen RNAsey plus mini kit following the manufacturer's instructions. Before loading the lysate onto RNAsey plus columns, the cell lysate was passed through QIAshredder columns to ensure complete homogenization and removal of polymer debris and clumps.

Total RNA was quantified using Agilent RNA nanochips in Bioanalyzer 2100. RNA samples with RIN values > 8 were used for library preparation. An exon junction assay was performed using an intron spanning GAPDH primer to generate an amplicon size of 500 bp ensuring the functionality of RNA molecules before library preparation. The integrity and functionality checked RNA samples were shipped to GeneCore, EMBL Heidelberg for library preparation and sequencing in low bind RNA tubes (Eppendorf).

4.18. Library preparation and sequencing

Barcoded stranded mRNA-seq libraries were prepared from total RNA (~200 ng) using the Illumina TruSeq stranded mRNA Sample Preparation v2 Kit (Illumina, San Diego, CA, USA) implemented on the liquid handling robot Beckman FXP2. Obtained libraries that passed the QC step were pooled in equimolar amounts; 1.8 pM solution of this pool was loaded on the Illumina sequencer NextSeq 500 and sequenced unidirectionally, generating ~500 million reads, each 85 bases long. The resulting fastq files were aligned to human genome v38, and Illumina sequencing adaptors were trimmed using the STAR sequence alignment tool.

The resulting aligned. bam files were used to extract UCSC annotated transcript counts using the R (V3.5) Bioconductor (V3.8) package TxDb. Hsapiens.UCSC.hg38. knownGene (V3.4.0). The counts data represents the number of sequence fragments representing each known gene for each sample.

4.19. Differential expression analysis

Once the transcript counts **Table**s were generated, Differential expression analysis was performed from the count matrix generated in the previous step using the R Bioconductor package DESeq2 (V1.22.2), which implements negative binomial distribution linear models to test differential expression. Differentially expressed genes (DEG) for each composite at each time point were calculated against undifferentiated hMSCs (TC-N) with an FDR cut-off of 5 %. Results were arranged in ascending order of adjusted p-value of significance of fold change (p adj). To stabilize the variations in counts data before DEG calculation, two types of count transformations were implemented in the DESeq2 pipeline, the variance stabilization transformation (VST) and the regularized logarithmic transformation (Rlog). Rlog transformations were chosen for the current study. PCA and MDS plots were used to assess data quality.

4.20. Ingenuity pathway analysis (IPA)

IPA (Qiagen) analysis was performed to elucidate canonical pathways and upstream regulator functions, along with ontology analysis for diseases and functions. Top canonical pathways and enriched gene functions falling under osteoinduction, osteoconduction, cellular remodeling, growth factor binding, effects on extracellular matrix, angiogenesis, vasculogenesis, cell movement, metabolism, and inflammation were identified and explored in detail.

4.21. Gene set enrichment analysis (GSEA)

Gene set enrichment analysis was performed to understand the biological processes, cellular components, and molecular functions relating to the differentially expressed genes from each group at each time point. Enriched biological functions were analyzed using a Web-based gene set analysis toolkit (webgestalt). Enriched functions were plotted based on their Normalized Enrichment Score (NES). A false discovery rate (FDR) of 0.05 was used for the analysis. A positive enrichment score represents activation of a function, while a negative enrichment score represents inhibition of a function.

4.22. In vivo metaphyseal implantation study

For the preclinical study, female skeletally mature (3+ years of age) sheep (*Ovis aries*) of 70–90 kg were used as the animal model due to their similar knee/joint and ACL shape and length anatomy to humans. The animals were treated with control and POC-HA femoral and tibial screws and allocated at time points of 3 and 6 months for a total of 24 animals. Each animal was treated with tibial and femoral interference screws to fix the implanted long digital extensor tendon graft, which was selected to replace the animal's removed ACL ligament. The screws allocated for histological analysis were also scanned with microCT to assess bone regeneration. A second animal study was conducted, including 6 animals treated only with POC-HA tibial and femoral screws for time points of 12 and 24 months, with the latter being extended to 36 months after compliance amendments. It must be mentioned that one animal unexpectedly died at 31 months instead of the 36-month group to which it was allocated. The data are included in the 36-month group for analysis. Sheep knee joints were excised, and microCT analysis and histology processing/histomorphometry imaging were performed.

Two open polygon ROIs were selected for the analysis of the microCT images. One ROI contained the tissue cavity, and the second contained the implant, as shown in Supplementary Fig. 5. To assess the closure of the wound due to bone formation, a ratio of the two ROIs (implant/tissue cavity) was calculated and expressed as a percentage. A lower percentage would denote lower cavity closure, thus healing in the anatomical area, whereas a higher percentage would denote an improved healing process.

For image analysis, 100 images from every ovine patient were analyzed, and the average value of their ratio was used for statistical purposes. Due to some time points having less than the minimum of N = 3 animals, femur and tibia ROI ratios were pooled together for a more robust statistical sample size. The first time points of 3 and 6 months, which included both control and POC-HA implants, were compared with a 2-way ANOVA test to evaluate the impact of time and treatment on bone healing.

Since POC-HA implants were studied until 36 months, a Kruskal-Wallis non-parametric test was used to investigate the effect of time in the wound regeneration, followed by Mann-Whitney U tests to identify statistical significance between different groups of interest ($p < 0.05$). Two donor image groups were excluded from the analysis due to their low-quality imaging for identifying ROIs. As a result, for the POC-HA implants, the following number of donors were used: 3 months (N = 6), 6 months (N = 6), 12 months (N = 3), 36 months (N = 4).

4.23. Histological assessment of regeneration

For the histological assessment, bony samples were cut lengthwise down the center of the test article, with one half used for decalcified slide preparation and the other half used for undecalcified slide preparation. Both types of tissue samples were fixed in 10 % neutral buffered formalin, but a different process was selected for each sample type.

Tissue samples were decalcified with 8 % trifluoroacetic acid at room temperature, processed by standard paraffin techniques, cut at 5 μm, and stained with Hematoxylin and Eosin (H&E). Undecalcified samples were infiltrated and polymerized into a hardened plastic block (Acrylosin Hard, Dorn and Hart Microedge Inc., Loxley, AL), stained with Sanderson's Rapid Bone stain to identify differentiated cells and cartilage areas, and then counterstained with Van Gieson stain, which detects bone and differentiated collagen.

Organ and adjacent soft tissue samples were processed by standard paraffin techniques, cut at 5 μm, and stained with H&E. The timepoints used for histology of both control and POC-HA samples were 0 months, 3 months, and 6 months, and POC-HA only at 12 months.

4.24. Destructive biomechanical analysis

Surgically treated knee joints were trimmed at the proximal end of the femur and the distal tibia, leaving the collateral soft tissue ligament across the joint. Samples were kept hydrated via physiologic saline spray at approximately 10-min intervals during the entire preparation protocol. The collateral ligaments were transected, and the joint capsule opened. The PCL tendon was cut. The ACL tendon was cut as close as possible to the articulating surface of the bone (i.e., the tibia or femur) containing the screw allocated to histology (Supplementary Fig. 4). This fine dissection process created two (n = 2) constructs from each sample: one for destructive biomechanics (i.e., the screw-tendon construct embedded in the bone plus the tendon graft length) and one for histology (i.e., the screw-tendon construct embedded in the bone). For samples allocated to destructive biomechanics, the bone of interest was potted within a PVC sleeve using a two-part epoxy resin (Smooth Cast 321, Smooth-on Inc. Easton, Pennsylvania). Prior to potting, several screws were drilled into both the proximal and distal portions of the bone to increase the purchase of the bone within the potting sleeve. The width and thickness of each tendon were measured using a caliper, and the cross-sectional area (CSA; mm^2) of each tendon was calculated by assuming a standard ellipse shape (Eq. (2)). CSA information was utilized to transform force data into the stress space.

Equation 2:

$$A = \pi * \text{width} * \text{thickness} \quad (2)$$

Specimens were mounted into the testing frame (Mini Bionix 858, MTS Systems, Eden Prairie, MN) using specially designed fixtures attached to a 5000 N (N) capacity force transducer (Supplementary Fig. 4). An upper fixture grip attached to the MTS machine's actuator was used to clamp onto the ACL tendon. Solid carbon dioxide was laid around the clamp to convert it into a cryo-clamp, lowering the temperature to at least −10 °C for biomechanical testing. Cryo-clamp temperature was monitored with a thermocouple (Model 52 II, Fluke Corporation, Everett, WA). Specimen hydration was maintained during testing via ambient temperature physiologic saline spray approximately every 10 min.

Destructive biomechanical testing included two phases: (A) preconditioning and (B) ramp to failure. Ramp to failure is a destructive test performed as the last test in the evaluation sequence. All loads imparted on the samples were applied quasi-statically and aligned collinearly to the physiologic loading direction of the tendon. All samples were loaded in the same approximate orientation with respect to bone and tendon orientation.

To minimize the viscoelastic effects on the measured biomechanical response, five (n = 5) cyclic tensile loads ranging between 0 and 2 % strain were applied to precondition the tendon. A ~2-min preload phase preceded the preconditioning phase. A static preload of 10 N was applied to all specimens for ~2 min or until the specimen was fully relaxed. The sample's reference gauge length was measured as the tendon's distance, in millimeters, from the bottom of the cryo-clamp's grip to the tendon's insertion into the bone (i.e., the tibia or femur) following the 10 N preload. The sample's reference gauge length was used to transform displacement data into the strain space.

To characterize the structural and material properties of the repaired

tissue, the specimens were quasi-statically loaded to failure at a rate of 0.5 % strain/sec. Load and displacement data were acquired at 100 Hz. Digital videos were collected during ramp-to-failure testing for failure mode analyses.

Ethics approval and consent to participate

All animal experiments performed at Colorado State University were approved by the Colorado State University Institutional Animal Care and Use Committee under approval #16-6981A.

CRediT authorship contribution statement

Arun Thirumaran: Investigation. **Meletios-Nikolaos Doulgkeroglou:** Validation, Methodology, Investigation, Formal analysis. **Magesh Sankar:** Methodology, Investigation, Formal analysis. **Jeremiah T. Easley:** Methodology, Investigation, Data curation. **Ben Gadomski:** Methodology, Investigation, Data curation, Conceptualization. **Anup Poudel:** Writing – original draft, Validation, Methodology, Investigation. **Manus Biggs:** Writing – original draft, Validation, Supervision, Resources, Project administration, Investigation, Funding acquisition, Data curation, Conceptualization.

Declaration of competing interest

A single researcher who participated in this study was partly funded by Acuitive Technologies Ltd. The in vivo portion of this study was funded by a research grant from Acuitive Technologies Ltd.

Acknowledgments

This work was funded through Science Foundation Ireland (SFI) and the European Regional Development Fund (Grant No. 13/RC/2073). The authors would like to acknowledge Genecore EMBL, REMEDI University of Galway, TRF University of Galway, the Genomics core facility at the University of Galway, and the Flow cytometry Core facility at the University of Galway. The authors also acknowledge the facilities and scientific and technical assistance of the Center for Microscopy & Imaging at the National University of Ireland Galway.

Appendix ASupplementary data

Supplementary data to this article can be found online at https://doi.org/10.1016/j.bioactmat.2024.06.030.

References

[1] T. Albrektsson, C. Johansson, Osteoinduction, osteoconduction and osseointegration, Eur. Spine J. 10 (Suppl 2) (2001) S96–S101.
[2] Y. Zhou, D.W. Hutmacher, S.L. Varawan, T.M. Lim, In vitro bone engineering based on polycaprolactone and polycaprolactone–tricalcium phosphate composites, Polym. Int. 56 (3) (2007) 333–342.
[3] S. Lohfeld, S. Cahill, V. Barron, P. McHugh, L. Dürselen, L. Kreja, C. Bausewein, A. Ignatius, Fabrication, mechanical and in vivo performance of polycaprolactone/tricalcium phosphate composite scaffolds, Acta Biomater. 8 (9) (2012) 3446–3456.
[4] X. Shao, J.C. Goh, D.W. Hutmacher, E.H. Lee, G.E. Zigang, Repair of large articular osteochondral defects using hybrid scaffolds and bone marrow-derived mesenchymal stem cells in a rabbit model, Tissue Eng. 12 (6) (2006) 1539–1551.
[5] M. Fini, G. Giavaresi, N.N. Aldini, P. Torricelli, R. Botter, D. Beruto, R. Giardino, A bone substitute composed of polymethylmethacrylate and α-tricalcium phosphate: results in terms of osteoblast function and bone tissue formation, Biomaterials 23 (23) (2002) 4523–4531.
[6] S.H. Li, J.R. De Wijn, P. Layrolle, K. De Groot, Synthesis of macroporous hydroxyapatite scaffolds for bone tissue engineering, J. Biomed. Mater. Res.: Off. J. Soc. Biomater. Japan. 61 (1) (2002) 109–120.
[7] L. Zou, Y. Zhang, X. Liu, J. Chen, Q. Zhang, Biomimetic mineralization on natural and synthetic polymers to prepare hybrid scaffolds for bone tissue engineering, Colloids Surf. B Biointerfaces 178 (2019) 222–229.
[8] G. Narayanan, V.N. Vernekar, E.L. Kuyinu, C.T. Laurencin, Poly (lactic acid)-based biomaterials for orthopaedic regenerative engineering, Adv. Drug Deliv. Rev. 107 (2016) 247–276.
[9] A. Kumar, S.M. Mir, I. Aldulijan, A. Mahajan, A. Anwar, C.H. Leon, A. Terracciano, X. Zhao, T.L. Su, D.M. Kalyon, S.G. Kumbar, Load-bearing biodegradable PCL-PGA-beta TCP scaffolds for bone tissue regeneration, J. Biomed. Mater. Res. B Appl. Biomater. 109 (2) (2021) 193–200.
[10] J.H. Shim, J.B. Huh, J.Y. Park, Y.C. Jeon, S.S. Kang, J.Y. Kim, J.W. Rhie, D.W. Cho, Fabrication of blended polycaprolactone/poly (lactic-co-glycolic acid)/β-tricalcium phosphate thin membrane using solid freeform fabrication technology for guided bone regeneration, Tissue Eng. 19 (3–4) (2013) 317–328.
[11] J.C. Kleinschmidt, L.J. Marden, D. Kent, N. Quigley, J.O. Hollinger, A multiphase system bone implant for regenerating the calvaria, Plast. Reconstr. Surg. 91 (4) (1993) 581–588.
[12] M. Cai, H. Liu, Y. Jiang, J. Wang, S. Zhang, A high-strength biodegradable thermoset polymer for internal fixation bone screws: preparation, in vitro and in vivo evaluation, Colloids Surf. B Biointerfaces 183 (2019) 110445.
[13] L.S. Nair, C.T. Laurencin, Biodegradable polymers as biomaterials, Prog. Polym. Sci. 32 (8–9) (2007) 762–798.
[14] P. Törmälä, J. Vasenius, S. Vainionpää, J. Laiho, T. Pohjonen, P. Rokkanen, Ultra-high-strength absorbable self-reinforced polyglycolide (SR-PGA) composite rods for internal fixation of bone fractures: in vitro and in vivo study, J. Biomed. Mater. Res. 25 (1) (1991) 1–22.
[15] K.A. Athanasiou, C.M. Agrawal, F.A. Barber, S.S. Burkhart, Orthopaedic applications for PLA-PGA biodegradable polymers, Arthrosc. J. Arthrosc. Relat. Surg. 14 (7) (1998) 726–737.
[16] O. Böstman, H. Pihlajamäki, Clinical biocompatibility of biodegradable orthopaedic implants for internal fixation: a review, Biomaterials 21 (24) (2000) 2615–2621.
[17] J.C. Middleton, A.J. Tipton, Synthetic biodegradable polymers as orthopedic devices, Biomaterials 21 (23) (2000) 2335–2346.
[18] R.T. Tran, L. Wang, C. Zhang, M. Huang, W. Tang, C. Zhang, Z. Zhang, D. Jin, B. Banik, J.L. Brown, Z. Xie, Synthesis and characterization of biomimetic citrate-based biodegradable composites, J. Biomed. Mater. Res. 102 (8) (2014) 2521–2532.
[19] J. Yang, A.R. Webb, S.J. Pickerill, G. Hageman, G.A. Ameer, Synthesis and evaluation of poly (diol citrate) biodegradable elastomers, Biomaterials 27 (9) (2006) 1889–1898.
[20] H. Qiu, J. Yang, P. Kodali, J. Koh, G.A. Ameer, A citric acid-based hydroxyapatite composite for orthopedic implants, Biomaterials 27 (34) (2006) 5845–5854.
[21] S.H. Rhee, J. Tanaka, Effect of citric acid on the nucleation of hydroxyapatite in a simulated body fluid, Biomaterials 20 (22) (1999) 2155–2160.
[22] E.J. Chung, P. Kodali, W. Laskin, J.L. Koh, G.A. Ameer, Long-term in vivo response to citric acid-based nanocomposites for orthopaedic tissue engineering, J. Mater. Sci. Mater. Med. 22 (2011) 2131–2138.
[23] Y.Y. Hu, A. Rawal, K. Schmidt-Rohr, Strongly bound citrate stabilizes the apatite nanocrystals in bone, Proc. Natl. Acad. Sci. USA 107 (52) (2010) 22425–22429.
[24] T. Yoshikawa, H. Ohgushi, S. Tamai, Immediate bone forming capability of prefabricated osteogenic hydroxyapatite, J. Biomed. Mater. Res. 32 (3) (1996) 481–492.
[25] E.J. Chung, M.J. Sugimoto, G.A. Ameer, The role of hydroxyapatite in citric acid-based nanocomposites: surface characteristics, degradation, and osteogenicity in vitro, Acta Biomater. 7 (11) (2011) 4057–4063.
[26] Y. He, Q. Li, C. Ma, D. Xie, L. Li, Y. Zhao, D. Shan, S.K. Chomos, C. Dong, J. W. Tierney, L. Sun, Development of osteopromotive poly (octamethylene citrate glycerophosphate) for enhanced bone regeneration, Acta Biomater. 93 (2019) 180–191.
[27] J. Guo, X. Tian, D. Xie, K. Rahn, E. Gerhard, M.L. Kuzma, D. Zhou, C. Dong, X. Bai, Z. Lu, J. Yang, Citrate-based tannin-bridged bone composites for lumbar fusion, Adv. Funct. Mater. 30 (27) (2020) 2002438.
[28] E.J. Chung, H. Qiu, P. Kodali, S. Yang, S.M. Sprague, J. Hwong, J. Koh, G.A. Ameer, Early tissue response to citric acid–based micro-and nanocomposites, J. Biomed. Mater. Res. 96 (1) (2011) 29–37.
[29] S.A. Mookerjee, M.D. Brand, Measurement and analysis of extracellular acid production to determine glycolytic rate, JoVE (106) (2015) e53464.
[30] Y. Kato, S. Ozawa, C. Miyamoto, Y. Maehata, A. Suzuki, T. Maeda, Y. Baba, Acidic extracellular microenvironment and cancer, Cancer Cell Int. 13 (2013) 1–8.
[31] C. Ma, X. Tian, J.P. Kim, D. Xie, X. Ao, D. Shan, Q. Lin, M.R. Hudock, X. Bai, J. Yang, Citrate-based materials fuel human stem cells by metabonegenic regulation, Proc. Natl. Acad. Sci. USA 115 (50) (2018) E11741–E11750.
[32] F. Dickens, The citric acid content of animal tissues, with reference to its occurrence in bone and tumour, Biochem. J. 35 (8–9) (1941) 1011.
[33] Y. He, Q. Li, C. Ma, D. Xie, L. Li, Y. Zhao, D. Shan, S.K. Chomos, C. Dong, J. W. Tierney, L. Sun, Development of osteopromotive poly (octamethylene citrate glycerophosphate) for enhanced bone regeneration, Acta Biomater. 93 (2019) 180–191.
[34] R.T. Tran, L. Wang, C. Zhang, M. Huang, W. Tang, C. Zhang, Z. Zhang, D. Jin, B. Banik, J.L. Brown, Z. Xie, Synthesis and characterization of biomimetic citrate-based biodegradable composites, J. Biomed. Mater. Res. 102 (8) (2014) 2521–2532.
[35] C. Ma, X. Tian, J.P. Kim, D. Xie, X. Ao, D. Shan, Q. Lin, M.R. Hudock, X. Bai, J. Yang, Citrate-based materials fuel human stem cells by metabonegenic regulation, Proc. Natl. Acad. Sci. USA 115 (50) (2018) E11741–E11750.
[36] J. Yang, A.R. Webb, G.A. Ameer, Novel citric acid-based biodegradable elastomers for tissue engineering, Adv. Mater. 16 (6) (2004) 511–516.

[37] S.A. Mookerjee, A.A. Gerencser, D.G. Nicholls, M.D. Brand, Quantifying intracellular rates of glycolytic and oxidative ATP production and consumption using extracellular flux measurements, J. Biol. Chem. 292 (17) (2017) 7189–7207.
[38] S.A. Mookerjee, R.L. Goncalves, A.A. Gerencser, D.G. Nicholls, M.D. Brand, The contributions of respiration and glycolysis to extracellular acid production, Biochim. Biophys. Acta Bioenerg. 1847 (2) (2015) 171–181.
[39] E. Bagnoli, T. Diviney, U. FitzGerald, Dysregulation of astrocytic mitochondrial function following exposure to a dopamine metabolite: implications for Parkinson's disease, Eur. J. Neurosci. 53 (9) (2021) 2960–2972.